Benchmark Supercritical Wing Computations Using CREATE-AV KESTREL and NASA AEROM

Walter A. Silva*

NASA Langley Research Center, Hampton, Virginia

The Benchmark Supercritical Wing (BSCW) is a benchmark configuration under evaluation within the Aeroelastic Prediction Workshops (AePWs). This wing was tested in the NASA Transonic Dynamics Tunnel (TDT) as part of the Benchmark Models Program (BMP) in the 1990s and is expected to be tested again in the TDT in 2026. The data acquired during the BMP tests includes unsteady pressure data and aeroelastic responses at various Mach numbers, dynamic pressures, and angles of attack. At the higher angles of attack, the existence of significant unsteadiness and separated flow results in a challenging case for CFD-based aeroelastic predictions. The AePW workshops have focused on various parts of these BSCW test data and a recent major focus regards the higher angle-of-attack conditions. The NASA AEROM software is applied to this configuration at M=0.8 and several angles of attack to evaluate the capability of the method to capture nonlinear unsteady aerodynamic effects at the higher angles of attack. The AEROM software is applied via the CREATE-AV KESTREL CFD code and AEROM results are compared with results from the CREATE-AV KESTREL solutions.

I. Introduction

The Benchmark Supercritical Wing (BSCW) model, shown in Figure 1, has a simple, rectangular, 16- x 32-inch wing planform, with a NASA SC(2)-0414 airfoil. It was first tested in the TDT in 1991.[1] For this test, the wing was mounted on the TDT Pitch and Plunge Apparatus (PAPA) to obtain the flutter boundary at various Mach numbers and angles of attack for this two-degree of freedom (pitch and plunge) system. In 2000, the wing was tested again, this time on an Oscillating Turn Table (OTT).[2] The purpose of the OTT tests was to measure aerodynamic response during sinusoidal (forced) pitch oscillation of the wing. The experimental data indicated that the BSCW exhibited a strong shock and separated flow at moderate angles of attack at transonic conditions. The computations of the transonic flow, in conjunction with the flutter boundary predictions, were the focus of the second workshop.[3] The OTT test also provided some experimental data for the computational analysis of the shock-buffet environment. Specifically, before each forced oscillation test, the wing was set at a fixed angle of attack and the unsteady pressure data was collected.

For both the OTT and PAPA tests, the model was mounted to a strut and sufficiently offset from the wind-tunnel wall (40 inches) via a large splitter plate, to (1) place the wing closer to the tunnel centerline and (2) be outside the tunnel wall boundary layer,[4] as shown in Figure 2. The wing was designed to be rigid, with the following structural frequencies for the combined wing and OTT mounting system: 24.1 Hz (spanwise first bending mode), 27.0 Hz (in-plane first bending mode), and 79.9 Hz (first torsion mode). When installed on the PAPA mount, the combined system frequencies were 3.33 Hz for the plunge mode and 5.20 Hz for the pitch mode.[5] The plunge and pitch modes are the only modes considered in the aeroelastic analyses of the PAPA-mounted configuration. The dashed yellow line indicates location of boundary layer transition/trip strip.

For instrumentation, the model has pressure ports in chordwise rows at the 60% and 95% span locations, as shown in Figure 3. For the BSCW/PAPA test, both rows were fully populated with unsteady in situ pressure transducers. The quantitative information obtained consists of unsteady data at flutter points and averaged data on a rigidized apparatus at the flutter conditions. For the BSCW/OTT test, only the inboard

*NASA Emeritus Langley Associate, Aeroelasticity Branch, AIAA Fellow.

row at 60% span was populated with transducers. The quantitative information for the OTT test consists of unsteady pressure data and accelerometer data for forced pitch oscillations and for the static system at constant flow conditions. The analysis of the OTT experimental data is described in Reference.[6]

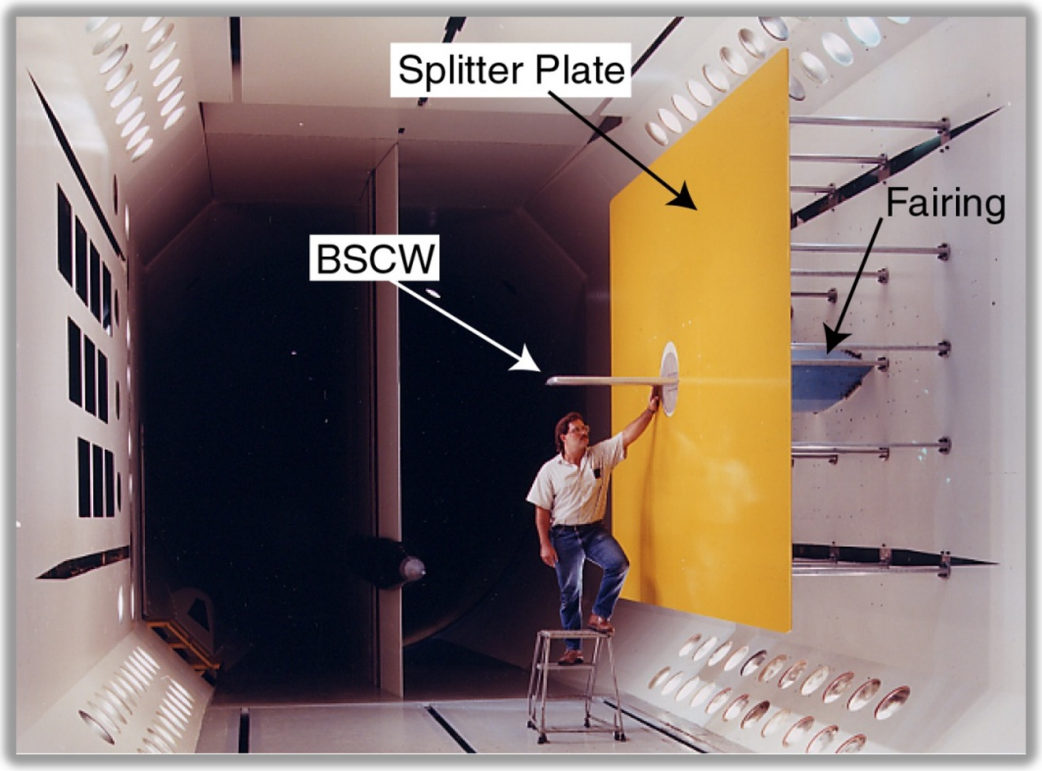

Figure 1: BSCW model mounted on the OTT in TDT.[7] Credit: NASA

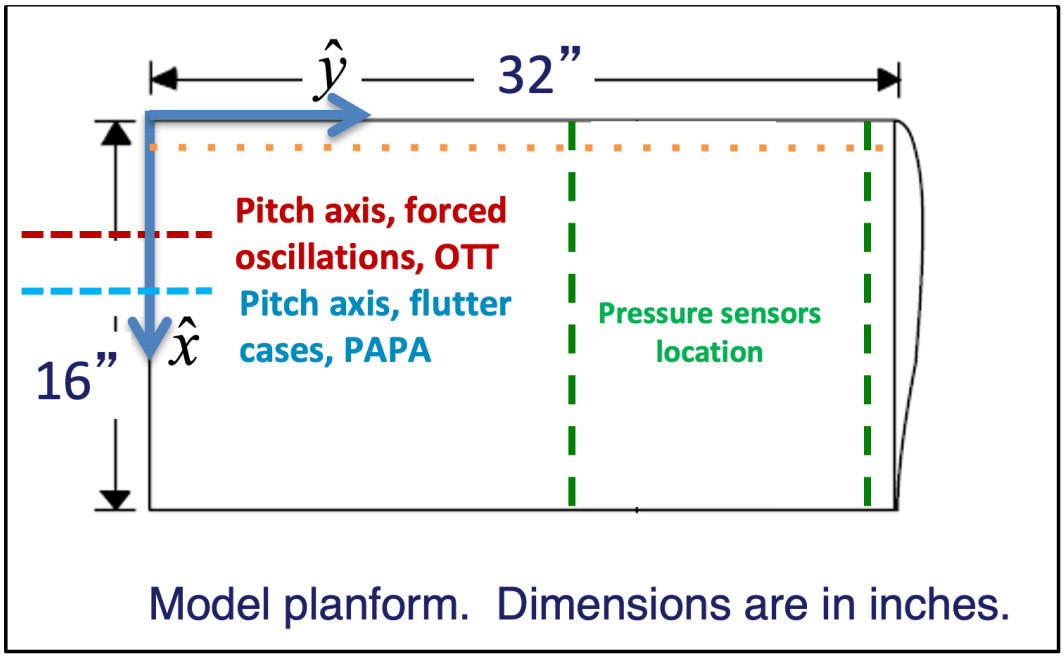

Figure 2: BSCW geometry details. Boundary layer transition strip shown as dotted yellow line.

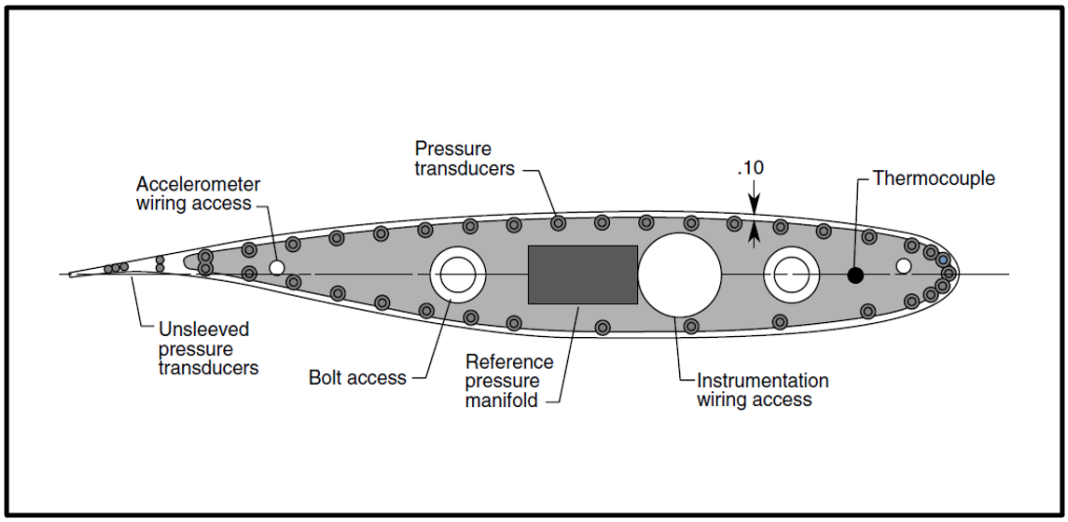

Figure 3: BSCW instrumentation: SC(2)-0414 airfoil.

II. Computational Methods

II.A. CREATE-AV/KESTREL Code

The present work makes use of KCFD, which is Kestrel's second-order, cell-centered, finite-volume unstructured fluid dynamics solver. KCFD solves both the steady and unsteady forms of the Reynolds-averaged Navier-Stokes (RANS) equations using either the Spalart-Allmaras (SA) one-equation turbulence model or the Menter two-equation turbulence model [8]. The SA model includes an optional rotational/curvature (RC) correction. The Menter model supports the "baseline" Menter model, the shear stress transport (SST) model, and a modified version of the SST model called "SSTM" [9]. Both models include an optional quadratic constitutive relation (QCR) extension, and both models support the improved delayed detached eddy simulation (IDDES) approach.

A modal structural solution is again utilized here, but rather than retaining only the first two modes (pitch and plunge), the first eighteen modes of the FEM[8] were retained, though only the first two PAPA modes exhibited aeroelastic response during the simulations. The modal-based structural dynamic solver (ModalSD) uses a predictor-corrector time integration scheme, in addition to a sub-iteration scheme similar to that used in KCFD in order to support sub-iteration data transfer between solvers. The forces are interpolated from the fluid mesh to the structural model and the displacements are interpolated from the structural model to the fluid surface using an infinite-plate spline. The first stage moves the nodes close to the deformed surface as "rigidly" as possible, and the second stage uses a surface influence scheme to relax the deformation into the volume. This approach is algebraic and has the advantage that the location of each node in the volume mesh is a function of the initial mesh and the current deformed surface mesh and does not depend on the mesh deformation history.

II.B. AEROM

In structural dynamics, the realization of discrete-time state-space models that describe the modal dynamics of a structure has been enabled by the development of algorithms such as the ERA[9] and the Observer Kalman Identification (OKID)[10] Algorithm. These algorithms perform state-space realizations by using the Markov parameters (discrete-time impulse responses) of the systems of interest. These algorithms have been combined into one package known as SOCIT[11] developed at NASA Langley Research Center.

There are several algorithms within the SOCIT that are used for the development of unsteady aerodynamic discrete-time state-space models. The PULSE algorithm is used to extract individual input/output impulse responses from simultaneous input/output responses. For a four-input/four-output system, simultaneous excitation of all four inputs yields four output responses. The PULSE algorithm is used to extract the individual sixteen (all combinations of four inputs and four outputs) impulse responses that associate

the response in each of the outputs due to each of the inputs. Once the individual sixteen impulse responses are available, they are then processed via the ERA in order to transform the sixteen individual impulse responses into a four-input/four-output, discrete-time, state-space model. A brief summary of the basis of this algorithm follows.

A finite dimensional, discrete-time, linear, time-invariant dynamical system has the state-variable equations

$$x(k+1) = Ax(k) + Bu(k) \tag{1}$$

$$y(k) = Cx(k) + Du(k) \tag{2}$$

where x is an n-dimensional state vector, u an m-dimensional control input, and y a p-dimensional output or measurement vector with k being the discrete time index. The transition matrix, A, characterizes the dynamics of the system. The goal of system realization is to generate constant matrices (A, B, C, D) such that the output responses of a given system due to a particular set of inputs is reproduced by the discrete-time state-space system described above.

For the system of Eqs. (1) and (2), the time-domain values of the discrete-time impulse responses of the system are also known as the Markov parameters and are defined as

$$Y(k) = CA^{k-1}B + D \tag{3}$$

with A an (n x n) matrix, B an (n x m) matrix, C a (p x n) matrix, and D an (p x m) matrix. The ERA algorithm begins by defining the generalized Hankel matrix consisting of the discrete-time impulse responses for all input/output combinations. The algorithm then uses the singular value decomposition to compute the (A, B, C, D) matrices.

In this fashion, the ERA is applied to unsteady aerodynamic impulse responses to construct unsteady aerodynamic state-space models. The AEROM software includes the necessary SOCIT routines as well as additional routines to manage the data flow and model generation.

II.B.1. AEROM Development Processes

The application of AEROM for the development of an aeroelastic ROM consists of two parts: the creation of the unsteady aerodynamic ROM and the creation of the structural dynamic ROM. The combination of the unsteady aerodynamic ROM with the structural dynamic ROM yields what is referred to as the aeroelastic simulation ROM.

An outline of the AEROM development process is as follows:

1. Generate the number of functions (from a selected family of orthogonal functions) that corresponds to the number of structural modes; for these analyses, the Walsh orthogonal functions were used as modal inputs;

2. Apply the generated input functions simultaneously via one CFD execution resulting in GAF responses due to these inputs; these responses are computed directly from the restart of a steady rigid CFD solution (not about a particular dynamic pressure);

3. Using the simultaneous input/output responses, identify the individual impulse responses using the PULSE algorithm (within SOCIT);

4. Transform the individual impulse responses generated in Step 3 into an unsteady aerodynamic state-space system using the ERA (within SOCIT);

5. Evaluate/validate the state-space models generated in Step 4 via comparison with CFD results (i.e., ROM results vs. full CFD solution results);

A schematic of steps 1-4 of the AEROM process outlined above is presented as Figure 4. Using modal information (generalized masses, modal frequencies, and modal dampings), a state-space model of the structure is generated. This state-space model of the structure is referred to as the structural dynamic ROM (see Figure 5). Once an unsteady aerodynamic ROM and a structural dynamic ROM have been generated, they are combined to form an aeroelastic simulation ROM (see Figure 6). Then root locus plots are extracted from the aeroelastic simulation ROM.

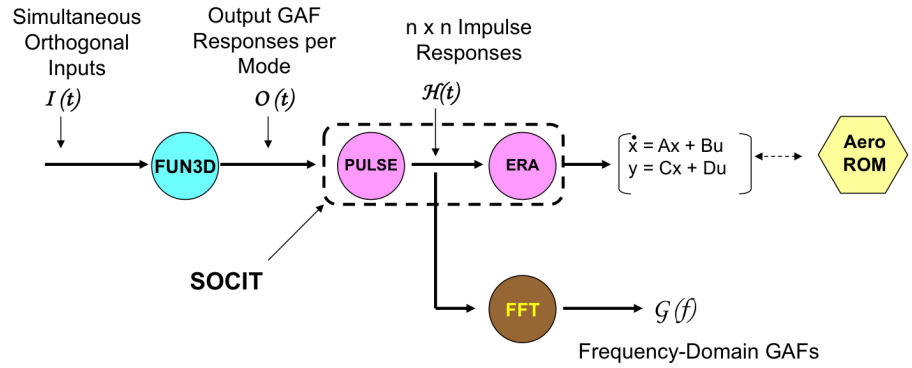

Figure 4: Process for generation of a linearized, unsteady aerodynamic state-space ROM (Steps 1-4).

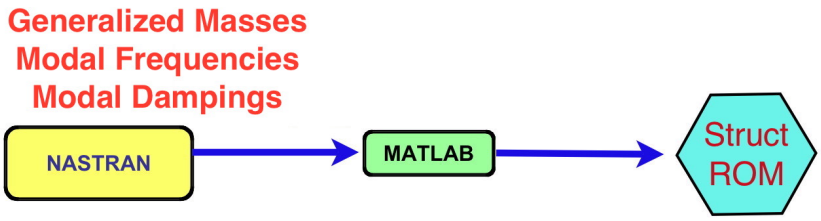

Figure 5: Process for generation of a linear structural dynamic state-space ROM.

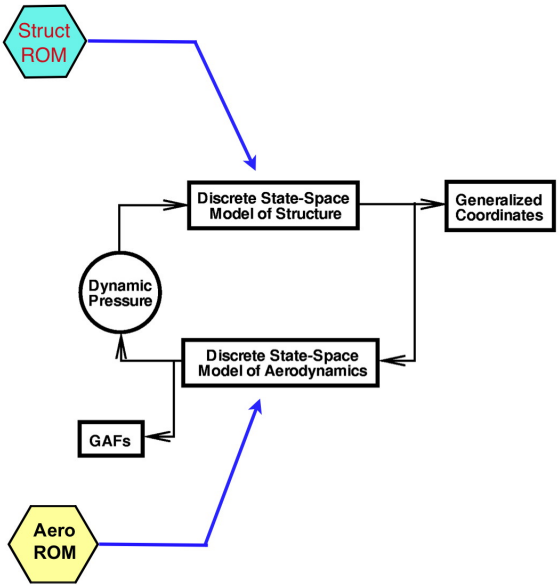

Figure 6: Process for generation of an aeroelastic simulation ROM consisting of an unsteady aerodynamic state-space ROM and a structural dynamic state-space ROM.

By design, the AEROM software enables a greater range of unsteady aerodynamic state-space model linearizations without imposing a more restrictive superposition (linear) assumption. This capability is implemented in two ways. First, the Walsh modal generalized coordinate inputs are applied simultaneously, regardless if the inputs consist of two modes or 100 modes. By applying all inputs simultaneously (i.e., not imposing a linear assumption of superposition by applying inputs separately), any possible input cross-terms, due to possible nonlinear effects, are included in the responses. Second, the modal amplitude of the Walsh input functions is adjustable in order to, again, excite possible nonlinear higher-order terms.

For this particular application of AEROM to the BSCW configuration, the effect of Walsh input function amplitudes is investigated, in particular, at the higher angles of attack where significant unsteady aerodynamic unsteadiness/separation, and therefore, nonlinearity, is exhibited. The results that follow will present the generation of different ROMs at each angle of attack as a function of Walsh input function amplitude and the resultant ROM predictions. These ROM models will be evaluated and compared with standard Kestrel solutions. Details of the AEROM software are available in the References.[12]

III. Results

Results consisting of comparisons between AEROM and KESTREL are presented in this section. In order to evaluate any amplitude-related effects using AEROM, models were developed at four different modal amplitudes at four different angles of attack as presented in Table 1. Corresponding KESTREL results were generated at the three angles of attack indicated: zero, three, and five degrees. The KESTREL results at one degree are not included as results were practically identical to results from zero degrees.

Table 1: AEROM solutions generated at four different modal amplitudes and four angles of attack. The (K) indicates corresponding KESTREL solutions at these conditions.

Modal Amplitude/Alpha (deg)	0 (K)	1	3 (K)	5 (K)
0.04	M8A0a	M8A1a	M8A3a	M8A5a
0.01	M8A0b	M8A1b	M8A3b	M8A5b
0.08	M8A0c	M8A1c	M8A3c	M8A5c
0.001	M8A0d	M8A1d	M8A3d	M8A5d

Presented in Figure 7 is a schematic showing the overall process for the creation of AEROM models using KESTREL for the BSCW. Since there are only two modes of interest, only two Walsh input functions are required. The result from a single KESTREL solution is indicated as the output generalized aerodynamic forces (GAFs). Clearly, because the inputs are applied simultaneously, there are only two corresponding outputs with each output containing contributions from each input. As presented in the previous section, in order to generate a linearized state-space model of the unsteady aerodynamic system, AEROM is used to extract the four corresponding impulse responses since the number of impulse responses for any system is equal to the number of inputs times the number of outputs (four, in this case).

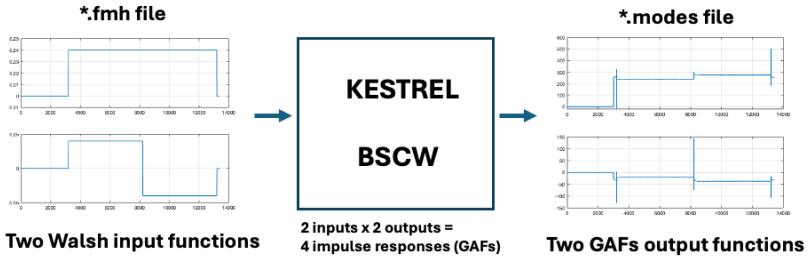

Figure 7: Application of simultaneous Walsh generalized coordinate modal input functions to Kestrel via the ".fmh" file and resultant generalized aerodynamic force responses in the ".modes" file. Two inputs and two outputs defines four unsteady aerodynamic impulse responses that are identified using AEROM.

The resultant GAFs output from KESTREL due to Walsh input functions will be presented to provide a measure of the accuracy of the AEROM model at a particular amplitude. The modal amplitudes are varied by varying the amplitude of the Walsh input functions since these functions define the amplitude and motions of the mode shapes being excited. Comparison of the AEROM GAFs with the KESTREL GAFs is used to assess relative accuracy as modal amplitudes are varied at each angle of attack. In addition, the variation of the aeroelastic root locus plots as a function of modal amplitude and angle of attack are presented as well. For brevity, only a subset of these results are included.

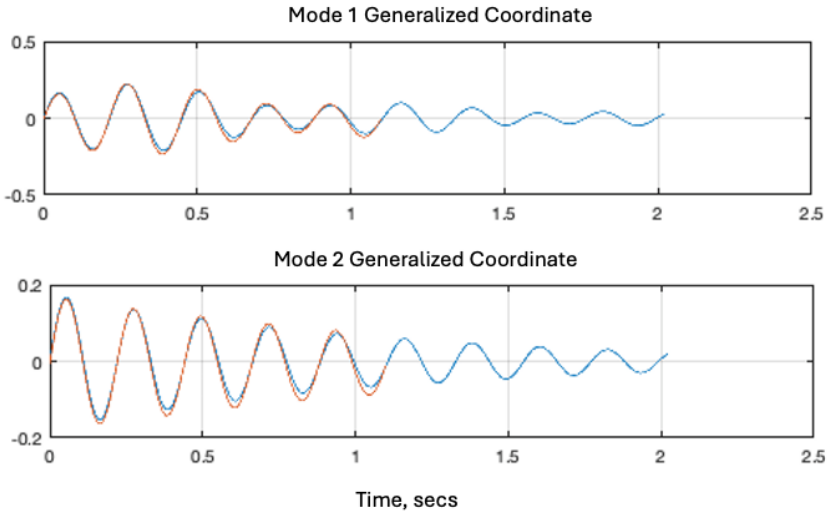

Figure 8: Comparison of modes 1 and 2 generalized coordinate responses between Kestrel (orange) and AEROM (blue) at M=0.80, alpha=0 deg, and Q=100 psf (M8A0a).

Presented in Figure 8 is a comparison of the AEROM and KESTREL generalized coordinates for the two modes at M=0.80, alpha=0 deg., and a dynamic pressure of 100 psf. As can be seen, the comparison is excellent with the AEROM able to accurately reproduce the KESTREL solution. At zero degrees angle of

attack, due to the benign (predominantly linear) flow conditions, there are no discernible differences in the accuracy of responses as modal amplitude is varied.

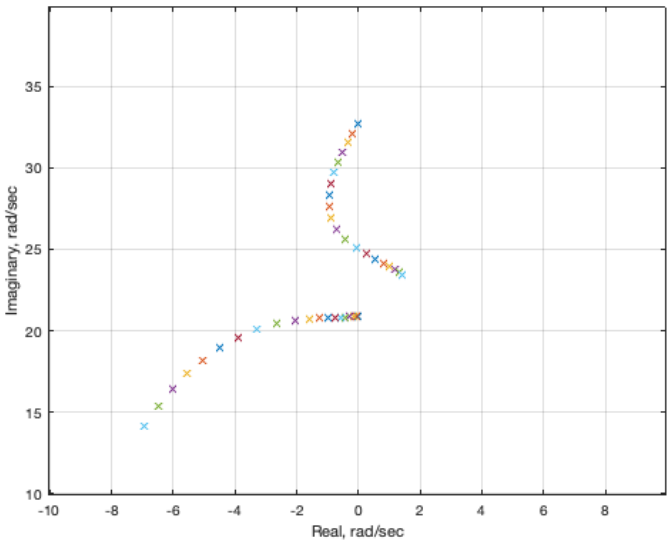

Figure 9: AEROM-generated aeroelastic root locus plot as a function of increasing dynamic pressure from 0 to 200 psf for the first amplitude (M8A0a) at M=0.80, alpha=0 deg.

Figure 9 presents the aeroelastic root locus plot generated by AEROM showing the coalescence of the two modes leading to a flutter condition when the imaginary axis is crossed. This plot is essentially unchanged at zero degrees angle of attack for all amplitude variations. Again, this is a strong indication that the unsteady aerodynamic responses at this condition are predominantly linear and insensitive to changes in modal amplitudes of excitation.

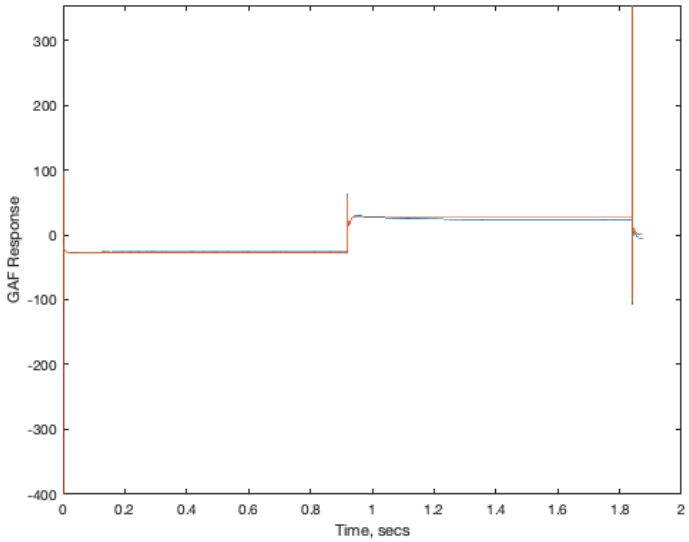

Figure 10: Comparison of AEROM and KESTREL mode 1 GAF due to Walsh input with first amplitude (M8A3a) at M=0.80, alpha=3 deg.

Presented in Figure 10 is a comparison of AEROM and KESTREL mode 1 GAF due to Walsh input with first amplitude (M8A3a) at M=0.80, alpha=3 deg. At this higher angle-of-attack, the increased unsteadiness

and separation in the flow starts to have an amplitude-related effect on the ability of AEROM to capture the unsteady aerodynamics at this condition. While the comparison is still quite good, slight differences can be noticed between the AEROM and KESTREL GAF responses.

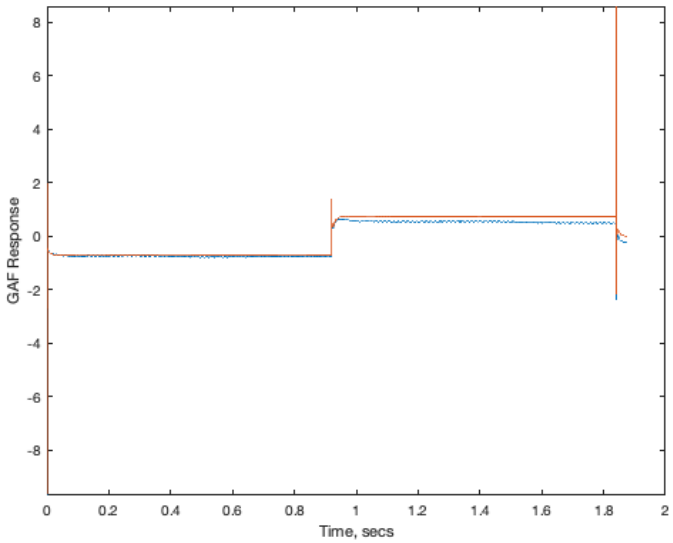

Figure 11: Comparison of AEROM and KESTREL mode 1 GAF due to Walsh input with fourth amplitude (M8A3d) at M=0.80, alpha=3 deg.

This difference in GAF responses as angle-of-attack is increased due to varying amplitudes is more noticeable in Figure 11. Using the AEROM model generated at an angle-of-attack of three degrees with the first amplitude, the resultant aeroelastic root locus plot is presented in Figure 12. Clearly, the increased level of nonlinear unsteady aerodynamic behavior results in a root locus plot that is quite different from the root locus plot presented for the zero degree angle-of-attack condition.

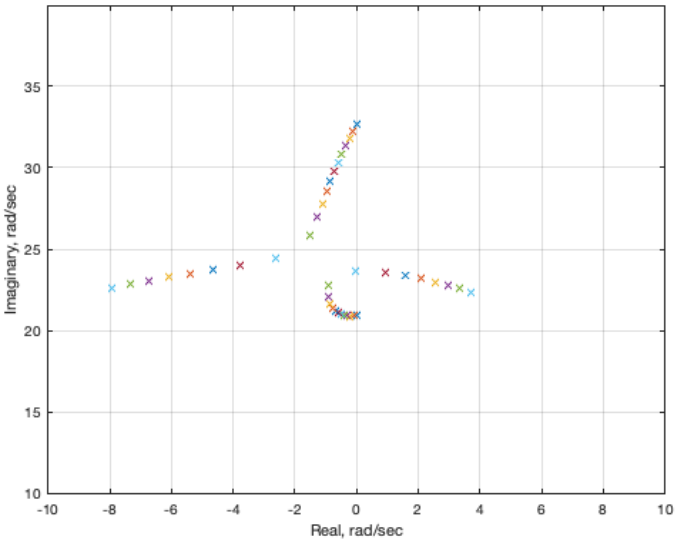

Figure 12: AEROM-generated aeroelastic root locus plot as a function of increasing dynamic pressure for the first amplitude (M8A3a) at M=0.80, alpha=3 deg.

Analysis of the results at angle-of-attack of five degrees indicates additional sensitivity to amplitude

variations. Presented in Figure 13 is a comparison of AEROM and KESTREL mode 1 GAF due to Walsh input with second amplitude (M8A5b) at M=0.80, alpha=5 deg. At this condition and amplitude, the discrepancy between the AEROM GAF and the KESTREL GAF is significant. The AEROM model based on this amplitude then yields the aeroelastic root locus plot presented in Figure 14 that is also significantly different from the aeroelastic root locus presented for the angle-of-attack of zero degrees condition.

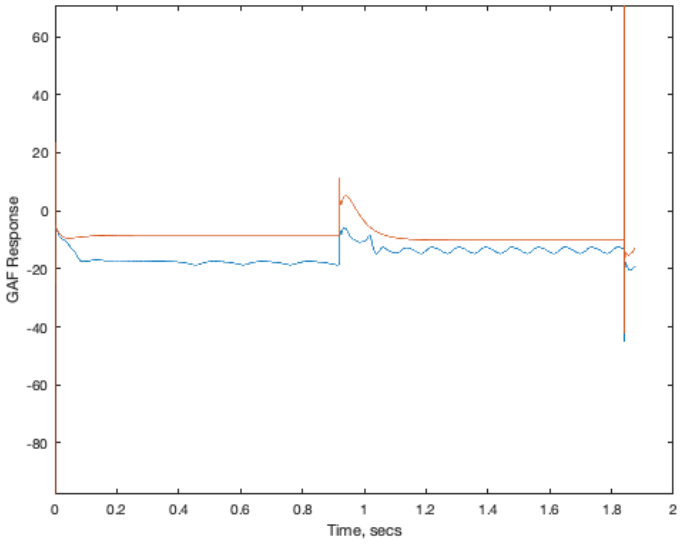

Figure 13: Comparison of AEROM and KESTREL mode 1 GAF due to Walsh input with second amplitude (M8A5b) at M=0.80, alpha=5 deg.

However, presented in Figure 15 is a comparison of AEROM and KESTREL mode 1 GAF due to Walsh input with third amplitude (M8A5c) at M=0.80, alpha=5 deg. At this amplitude, although there is a noticeable difference between the two results, the comparison is improved over the result due to the second amplitude. This indicates that an improved AEROM model can, in fact, be obtained if the system is excited at an appropriate modal amplitude that better captures a better portion of the relevant, complex unsteady aerodynamic responses.

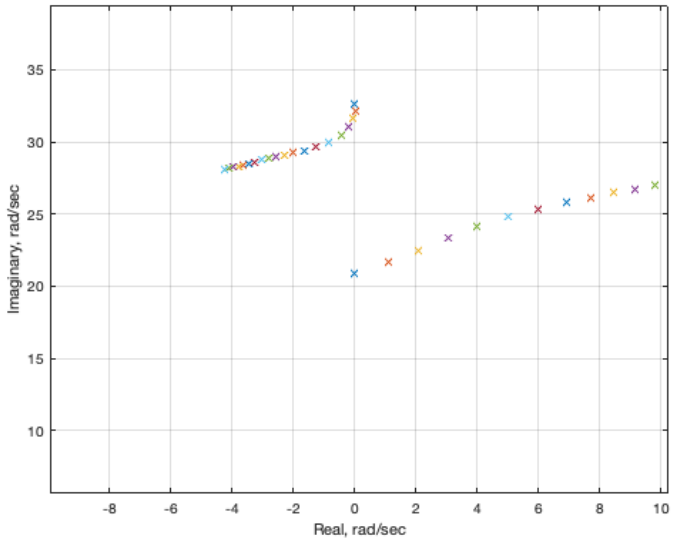

Figure 14: AEROM-generated aeroelastic root locus plot as a function of increasing dynamic pressure for the second amplitude (M8A5b) at M=0.80, alpha=5 deg.

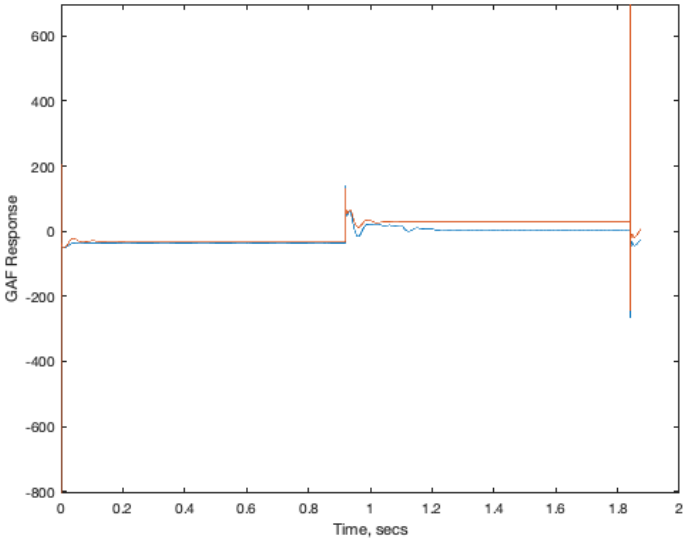

Figure 15: Comparison of AEROM and KESTREL mode 1 GAF due to Walsh input with third amplitude (M8A5c) at M=0.80, alpha=5 deg.

Similar comparisons can be made for the AEROM result based on the first amplitude (M8A5a). Presented in Figure 16 is a comparison of modes 1 and 2 generalized coordinate responses between Kestrel (orange) and AEROM (blue) for first amplitude (M8A5a) at M=0.80, alpha=5 deg, and a dynamic pressure of 50 psf. The comparison indicates good correlation between the AEROM prediction and the KESTREL solution. In Figure 17 is a similar comparison but at a higher dynamic pressure of 130 psf using the same AEROM model. These results indicate that the AEROM model generated using the larger amplitudes (amplitudes 1 and 3) can yield a reasonable AEROM model able to predict the aeroelastic responses generated by KESTREL that include significant unsteadiness and separated flow.

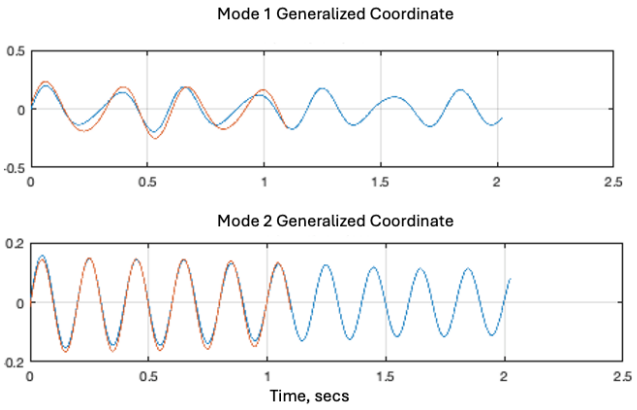

Figure 16: Comparison of modes 1 and 2 generalized coordinate responses between Kestrel (orange) and AEROM (blue) for first amplitude (M8A5a) at M=0.80, alpha=5 deg, and Q=50 psf.

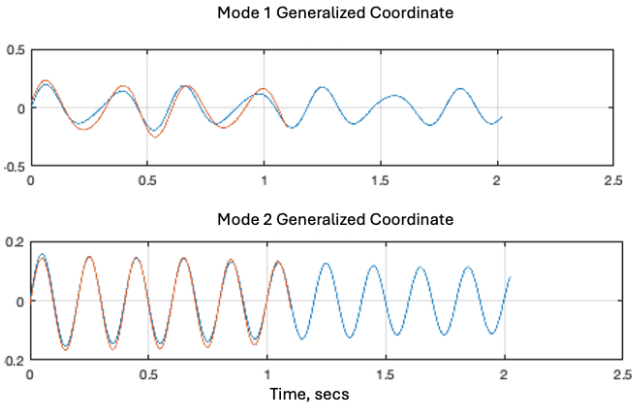

Figure 17: Comparison of modes 1 and 2 generalized coordinate responses between Kestrel (orange) and AEROM (blue) for the first amplitude (M8A5a) at M=0.80, alpha=5 deg, and Q=130 psf.

Finally, using the AEROM based on the first amplitude, the aeroelastic root locus plot generated from this model is presented in Figure 18. Of significant interest are two points. The first point is that this root locus plot is similar in nature to the root locus plot presented for angle-of-attack of zero degrees. The second point is that the second branch, due to the second mode, is significantly closer to the imaginary axis than the branch seen for the zero degree angle-of-attack case. This proximity to the imaginary axis is very important and revealing as it helps to explain the increased sensitivity to various parameters at this condition. That is, given this proximity to the imaginary axis, one CFD code with slightly different numerical damping characteristics (different flux limiter selection) could possible push this branch into the right-half plane, indicating a flutter instability. A different CFD code, with different numerical damping could maintain the branch on the left-half plane, maintaining aeroelastic stability. Therefore, as a result of using AEROM to investigate the nature of the aeroelastic responses as angle-of-attack is increased by applying varying modal amplitudes to the creation of these AEROM models, one can start to identify the potential source of aeroelastic stability at this highly unsteady aerodynamic condition with complex separated flow dynamics.

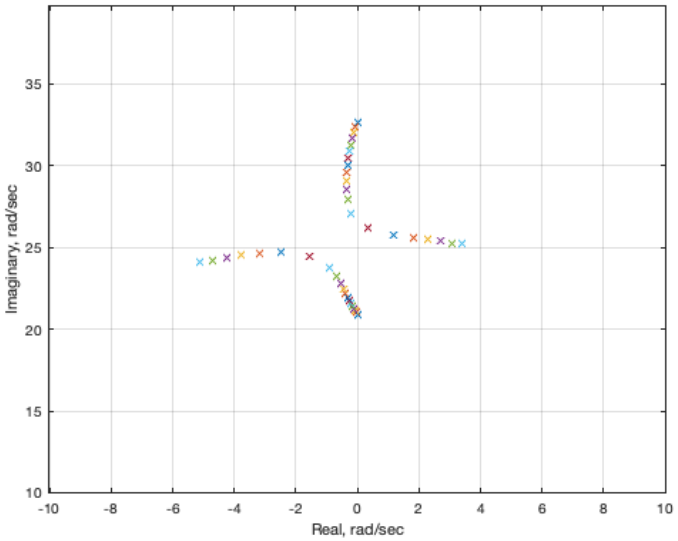

Figure 18: AEROM-generated aeroelastic root locus plot as a function of increasing dynamic pressure for the first amplitude at M=0.80, alpha=5 deg.

IV. Conclusions

The NASA AEROM software was applied to the Benchmark SuperCritical Wing (BSCW) using the CREATE-AV/KESTREL CFD code. Results were computed at M=0.8 at multiple angles of attack and several dynamic pressures. Two critical components of the AEROM software include: 1). the ability to excite all the modal inputs simultaneously via a single CFD solution, whether it be for two modes or 40 modes; and 2). the ability to vary the amplitude of the excitation inputs in order to excite higher-order nonlinear terms. Application of these two capabilities indeed demonstrates that input amplitude is very important to properly generate a good quality ROM at the higher angles of attack where the flow is highly unsteady/separated and is nonlinear. The results presented also included a comparison of the dynamic pressure aeroelastic root locus plots at each angle of attack condition. An important conclusion is that an aeroelastic root locus plot generated using AEROM models due to larger excitation Walsh modal inputs, at five degrees angle-of-attack, indicates that the root locus branch from the second mode shifted significantly towards the imaginary axis as compared with the root locus at zero degrees angle-of-attack. This proximity to the imaginary axis provides an explanation for the observed increased sensitivity of results, at this condition, from various CFD codes. Additional analyses are underway to compare these root locus plots for other CFD codes for confirmation of this interesting result.

References

[1]Dansberry, B. E., Durham, M. H., Bennett, Rivera, J. A., Silva, W. A., and Wieseaman, C. D., "Experimental Unsteady Pressures at Flutter on the Supercritical Wing Benchmark Model." AIAA Paper 1993-1592-CP, 1993.

[2]Piatak, D. J. and Cleckner, C. S., "A New Forced Oscillation Capability for the Transonic Dynamics Tunnel," AIAA Paper 2002-0171, Jan. 2002.

[3]Heeg, J., Wieseman, C. D., and Chwalowski, P., "Data Comparisons and Summary of the Second Aeroelastic Prediction Workshop," AIAA Paper 2016-3121, 2016.

[4]Schuster, D. M., "Aerodynamic Measurements on a Large Splitter Plate for the NASA Langley Transonic Dynamics Tunnel," NASA TM 2001-210828, March 2001.

[5]Dansberry, B. E., Durham, M. H., Bennett, R. M., Turnock, D. L., Silva, W. A., and Rivera, J. A., "Physical Properties of the Benchmark Models Program Supercritical Wing," NASA Technical Memorandum 4457, 1993.

[6]Heeg, J. and Piatak, D. J., "Experimental data from the Benchmark SuperCritical Wing wind tunnel test on an oscillating turntable," AIAA Paper 2013-1802, April 2013.

[7]Heeg, J., Chwalowski, P., Schuster, D. M., Dalenbring, M., Jirasek, A., Taylor, P., Mavriplis, D. J., Boucke, A., Ballmann, J., and Smith, M., "Overview and Lessons Learned from the Aeroelastic Prediction Workshop," IFASD Paper 2013-1A, 2013.

[8]Heeg, J., Chwalowski, P., Schuster, D. M., Raveh, D., Jirasek, A., and Dalenbring, M., "Plans and Example Results for the 2nd AIAA Aeroelastic Prediction Workshop," *56th AIAA/ASCE/AHS/ASC Structures, Structural Dynamics, and Materials Conference*, AIAA, January 2015.

[9]Juang, J.-N. and Pappa, R. S., "An Eigensystem Realization Algorithm for Modal Parameter Identification and Model Reduction," *Journal of Guidance, Control, and Dynamics*, Vol. 8, 1985, pp. 620–627.

[10]Juang, J.-N., Phan, M., Horta, L. G., and Longman, R. W., "Identification of Observer/Kalman Filter Markov Parameters: Theory and Experiments," *Journal of Guidance, Control, and Dynamics*, Vol. 16, 1993, pp. 320–329.

[11]Juang, J.-N., Horta, L. G., and Phan, M., "System Observer Controller Identification Toolbox," *NASA TM 19920015463*, 1992.

[12]Silva, W. A., "AEROM: NASA's Unsteady Aerodynamic and Aeroelastic Reduced-Order Modeling Software," *Aerospace*, Vol. 5(2), No. 41, 2018.